

We are IntechOpen, the world's leading publisher of Open Access books Built by scientists, for scientists

6,900

Open access books available

186,000

International authors and editors

200M

Downloads

Our authors are among the

154

Countries delivered to

TOP 1%

most cited scientists

12.2%

Contributors from top 500 universities



WEB OF SCIENCE™

Selection of our books indexed in the Book Citation Index
in Web of Science™ Core Collection (BKCI)

Interested in publishing with us?
Contact book.department@intechopen.com

Numbers displayed above are based on latest data collected.
For more information visit www.intechopen.com



The Study of Fabric Drying Using Direct-Contact Ultrasonic Vibration

Chang Peng and Saeed Moghaddam

Abstract

Our existing cloth drying technology is an energy-intensive process, which generally involves blowing hot air across tumbling wet fabrics to facilitate evaporation and moisture removal. To address the relatively low energy efficiency of existing cloth drying techniques, in this chapter, a totally new cloth drying technology is introduced, which uses high frequency ultrasonic vibrations generated by piezoelectric transducer instead of thermal heating to extract moisture in cloth as a cold mist, dramatically reducing drying time and energy consumption. The physical mechanism of ultrasonic fabric drying process in direct-contact mode is first studied. A novel ultrasonic transducer driving method, in which the power supply to the transducer is regulated by a binary modulating signal, is then developed for use in direct-contact ultrasonic drying of fabrics. A demonstration unit is finally fabricated to show the efficacy of the process and its energy saving compared to thermal drying process.

Keywords: fabric drying, energy efficiency, ultrasonic vibration, ultrasonic transducer, physical mechanism

1. Introduction

Clothes dryers offer a rapid means to dry laundry in households but consume substantial residential electricity. Clothes dryers are the second largest source of residential energy use in a household following water heater [1]. Every year the operation of clothes dryers in the United States consumes as much electricity as does the entire state of Massachusetts (60 billion kWh per year) [2]. The demand of clothes dryers in U.S. has increased by nearly 6% over the last decade. Until 2009, 80% of U.S. households had a clothes dryer and 80% of them are electric clothes dryers, the remaining being gas dryers [3]. Although a set of technologies such as air-vented dryers and heat pump dryers have been introduced to the market, the energy efficiency of clothes dryers has not been improved significantly over the last 20 years.

In the current clothes dryer architecture, the clothes dry by passing hot air over the wet fabric. The state of the art for clothes drying technology involves mechanical (centrifugal) water extraction in the washing machine followed by thermal drying in a dryer. The moisture initially extracted by the washing machine reduces the remaining moisture in the clothes to ~50% of the dry weight [4]. The clothes are then placed in a dryer drum, where the remaining moisture is removed by circulating heated air through them. Thermal water removal from clothes in all existing

Dryer type	Average drying time (min)	Energy factor (lb/kWh)
Electric standard (≥ 4.4 ft ³ capacity) [3]	40	3.73
Electric compact (120 V, ≤ 4.4 ft ³ capacity) [3]	40	3.61
Electric compact (240 V, ≤ 4.4 ft ³ capacity) [3]	35	3.27
Gas standard [3]	35	3.30
Heat pump [2]	82	7.6

Table 1.

Average clothes drying time and energy factor (EF) values for different types of commercialized clothes dryers.

dryer technologies [3, 5–10] (including heat, heat pump, vacuum, or microwave drying) requires a heat source to provide a latent heat of evaporation of about 2.5 MJ/kg water. The heat source for a dryer can be electric resistance, natural gas and/or an electric heat pump.

The metrics to measure the drying efficiency of a clothes dryer is called energy factor (EF), which commonly has three different types of definitions, depending on how the drying effect is qualified: (1) the mass of moisture removed per energy consumption; (2) the mass of cloth dried per energy consumption; or (3) the latent heat of moisture removed per energy consumption. In the United States, the Department of Energy standard of EF measures the mass of cloth (saturated to certain water content) that can be dried per unit of electricity consumed (lb/kWh) [3]. For gas dryers, it measures the pounds of clothes being dried per equivalent kilowatt-hour of natural gas consumed. Here, we focus on EF (lb/kWh) which is commonly used in the United States. **Table 1** summarizes the EF values for the typical types of existing clothes dryers.

Recently, for the first time, we have introduced a totally new cloth drying technology and are collaborating with Oak Ridge National Laboratory (ORNL) researchers to develop the world's first direct-contact ultrasonic cloth dryer that could potentially change the concept of residential heat-drying technology [11–15]. This novel approach uses high-frequency mechanical vibrations generated by piezoelectric ceramics instead of heat to extract moisture as a cold mist, dramatically reducing drying time and energy use. On the basis of inverse piezoelectric effect, when an electric field is applied in the polarization direction of piezoelectric ceramics, the ceramics will produce mechanical deformation in a certain direction. When a high frequency electric field is applied, the piezoelectric transducer generates acoustic vibration. If the oscillation frequency is larger than 20 kHz, it generates ultrasonic waves that propagate through its surrounding media [12, 16]. Coming to the studies reported on ultrasonic cloth drying per se, to our knowledge, Khmelev et al. [17, 18] is the only paper on this topic. However, a non-contact technique was used in their study, making our study unique and the first of its kind.

This study will address the feasibility of adopting the ultrasonic technique for cloth drying with the objective of achieving lower power consumption and process duration compared to the existing energy-intensive, thermal-based clothes dryers.

2. Experimental setup and method

A schematic of the experimental setup for studying both the water droplet atomization and the fabric drying process is shown in **Figure 1**. The setup mainly consists of six components: an ultrasonic transducer, a function generator, a power

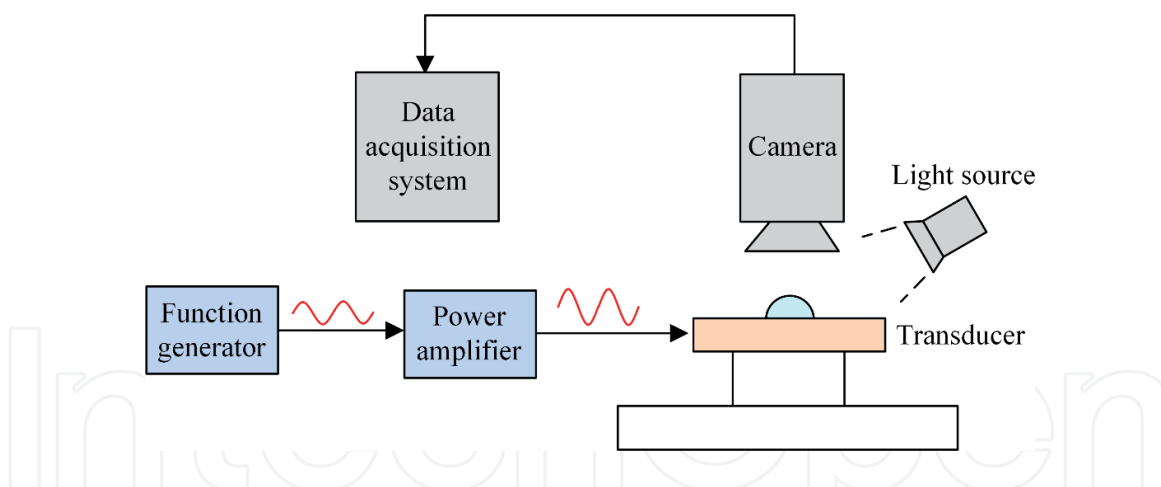


Figure 1.
 Schematic representation of the experimental setup for droplet atomization and fabric drying studies [11].

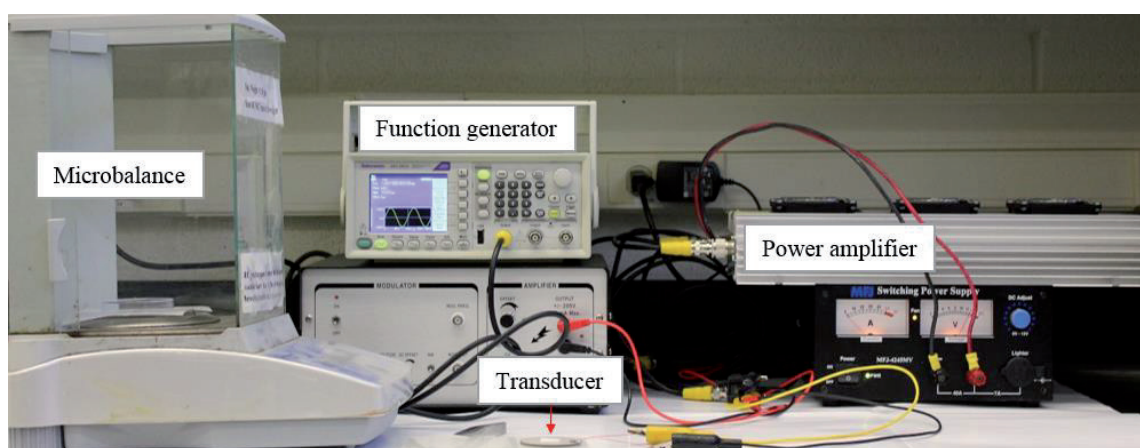


Figure 2.
 Experimental setup for fabric drying study [11].

Transducer	Working diameter (mm)	Resonant frequency (kHz)	Type
A	20	1600	Piezo crystal
B	50	1060	Piezo crystal
C	4.2	135	Metal mesh

Table 2.
 Parameters of transducers tested in this study [11].

amplifier, a high-speed camera, an infrared (IR) camera and a microbalance with a resolution of 0.1 mg for measuring the fabric weights. An image of the experimental setup is provided in **Figure 2**.

The detailed characteristics of the transducers tested in this study are summarized in **Table 2**. Transducer A and B are traditional piezoelectric transducers, the working surfaces of which consist of a piezoelectric ceramic, as shown in **Figure 3a–b**. Transducer C is a metal mesh-based transducer, which consists of a thin metal mesh sandwiched between two piezoelectric rings (**Figure 3c**) that vibrate the mesh. If a water droplet is in direct contact with the mesh surface, the metal mesh-based transducers allow water to pass through the mesh.

For the water droplet atomization study, a water droplet of a specified volume was deployed at the center of the transducer by using a micro-pipette. The atomization process was monitored using the high-speed camera at a frame rate of 3600

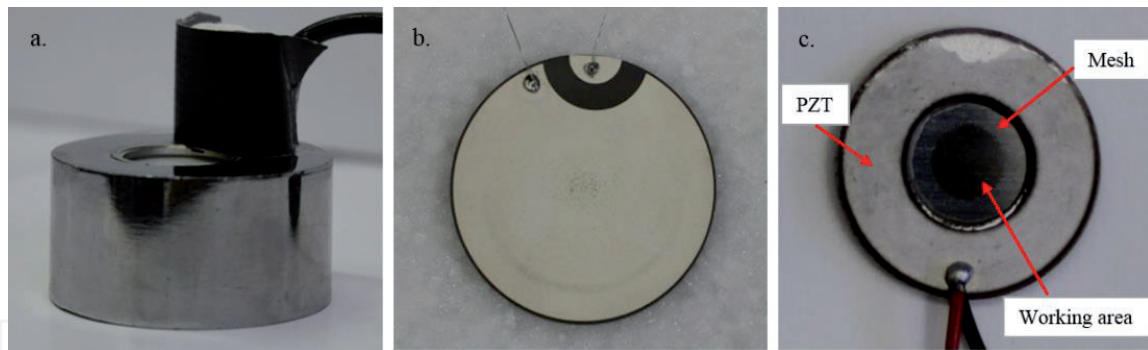


Figure 3. Images of the transducers used in this study: (a) transducer A, (b) transducer B, and (c) transducer C [11].

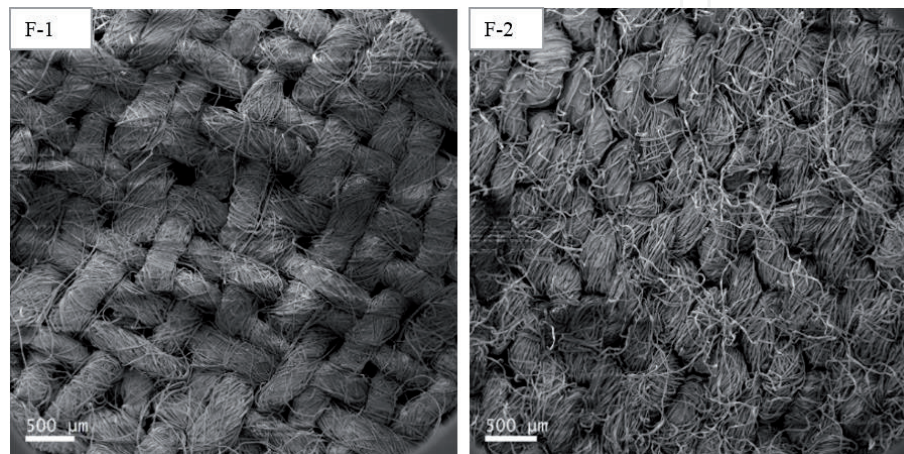


Figure 4. Scanning electron microscope images of the two DOE fabrics [11].

frames per second. The camera line of view was normal to the vibrating surface, thus providing top-view images of the atomizing droplets (**Figure 1**) [11]. During the water droplet atomization process, the IR camera was also used to monitor the droplet and transducer temperature changes. It was mounted in the same way as the high-speed camera. Trials were performed with the following values of the initial droplet volume: 10, 50, and 100 μL .

In the studies, two kinds of US Department of Energy (DOE) standard fabrics (hereinafter called F-1 and F-2) were tested. The SEM images of the fabrics are shown in **Figure 4**. As can be seen from **Figure 4**, F-1 has larger major pore sizes than F-2. Details on the contents, thicknesses and densities for these two fabrics can be found in Ref. [11].

In the studies, the microbalance, AL104, with an error of 0.1 mg was used to measure the weight of the saturated and unsaturated fabric samples to determine the volume of water remaining in the fabric. Prior to the drying test, the dry fabric was placed on the transducer and the weight of this system was measured on the microbalance. After this measurement, the fabric was wet with a known volume of water. The transducer was then actuated to begin the drying process. After 5 s elapsed, the transducer was turned off and the weight of the transducer-fabric system was measured. Immediately after this measurement, the fabric was completely dried by heating it to 80°C. The fabric was then rewet and the weight of the transducer-fabric system was measured after actuating the transducer for 10 s. The fabric was then completely dried. In this manner, the weight of an initially saturated transducer-fabric system was measured after actuating the transducer in increments of 5–10 s, with the fabric dried after each measurement. For each time

interval, the tests were repeated for at least three times. The measurements were recorded until the weight of the transducer-fabric system was less than 5% of the initially saturated system. This method of determining the drying rate of fabrics was repeated for the two fabrics on the three transducers.

3. Ultrasonic atomization of water droplet

Figure 5 illustrates the high-speed images recorded during the atomization of a 10 μL water droplet on transducer A. A qualitative analysis of these images can provide clues to the kinetics of the atomization process. In the initial stage after the transducer was turned on, the oscillations of the transducer surface were transmitted to the surface of the droplet resulting in the formation of capillary waves (**Figure 5b**). As time progressed, the capillary waves grew to form surface ligaments (**Figure 5c**), followed by the atomization of droplet (**Figure 5d–j**), which the droplet broke up via ejection of secondary droplets. The atomization of the droplet exhibited a very chaotic dynamic. In addition to the production of fine mist from the droplet surface, the droplet was observed to spread and deform during the process. [11].

The observed kinematics of droplet atomization can be explained by analyzing the relative magnitudes of the oscillation force (F_o) and surface tension force (F_s) influencing the process [11]. Assuming that the droplet forms a half-sphere on the transducer surface (**Figure 6**), the scale of F_o applied on the water droplet (droplet mass, m_{drop} , and density, ρ) can be presented as,

$$F_o \sim m_{drop} A \omega^2 \sim \frac{1}{12} \pi d^3 \rho A \omega^2 \quad (1)$$

where A and ω are the vibration amplitude and angular frequency ($\omega = 2\pi f$), respectively. On the other hand, the scale of the surface tension force (F_s) experienced by the droplet surface can be presented as [19],

$$F_s = \sigma \pi d \cos\theta \quad (2)$$

where σ is the liquid surface tension which is temperature (T) dependent; d is the droplet diameter which varies with time (t); and θ represents the contact angle formed at the liquid–solid interface.

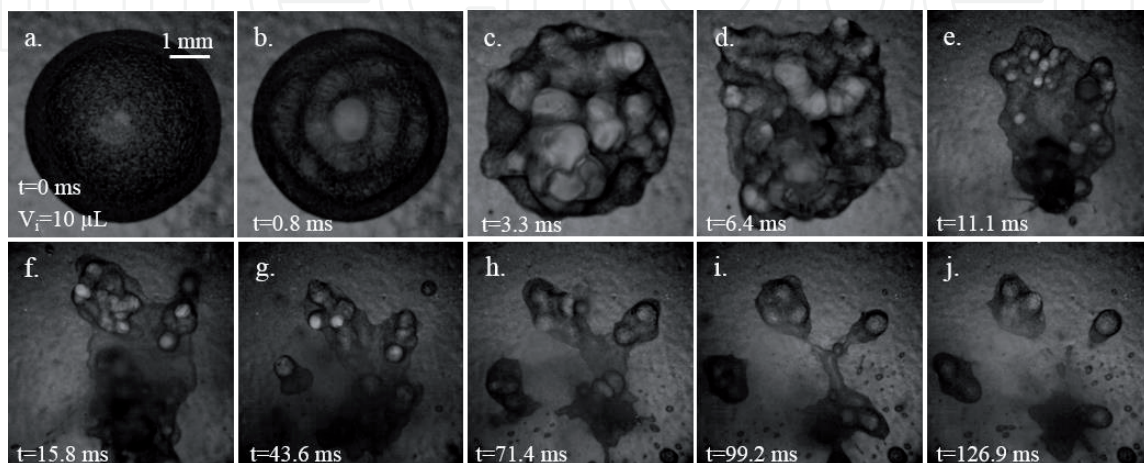


Figure 5. Different regimes of droplet atomization process on transducer A: (a) unperturbed droplet, (b) capillary wave regime, (c) ligament regime, and (d)–(j) catastrophic drop breakup and atomization [11].

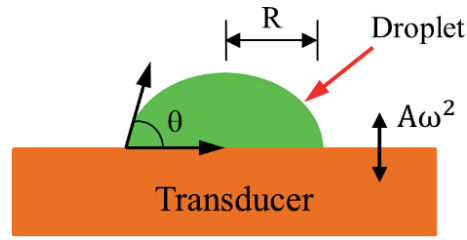


Figure 6.
Schematic of a water droplet on a vibrated transducer surface.

The relative magnitude of F_o and F_s can be expressed as,

$$R \sim \frac{F_o}{F_s} \sim \frac{d^2 \rho A \omega^2}{12 \sigma \cos \theta} \quad (3)$$

For a 10 μL water droplet on transducer A (**Figure 5a**), $F_o > F_s$ (i.e. $R > 1$) when the transducer was turned on. This caused the liquid–vapor interface to rupture (leading to atomization), reducing the droplet radius (r) and R . The atomization continued with time until $F_s > F_o$ (at a critical volume), at which point, the atomization process ceased.

During the ultrasonic droplet atomization process, the droplet temperature was also changed due to the viscous dissipation of continuous vibration. And as illustrated in Eq. 3, the surface tension of the droplet (σ) is temperature (T) dependent. Higher the droplet temperature, lower the surface tension will be. The lower surface tension will result in the lower surface tension force (F_s) (Eq. 3). In the following section, the temperature changes on the two types of transducers, piezoelectric crystal transducer and metal mesh transducer, were studied during the droplet atomization process.

Three different volumes of water, 10, 50, and 100 μL , were tested on transducers A, B and C. The thermal responses of these droplets were recorded using the IR camera and the maximum liquid temperature was extracted from this data. **Figure 7** presents the temporal variations in the maximum temperatures of these droplets on transducers. The x -axis represents a non-dimensional time (t^*) defined as

$$t^* = \frac{t}{t_0} \quad (4)$$

where t_0 represents the total duration of time that was recorded using the IR camera (**Tables 3 and 4**).

As can be seen from **Figure 7a**, the temperature for 10 μL droplet varied little immediately after the transducer A was actuated. The temperature went up to

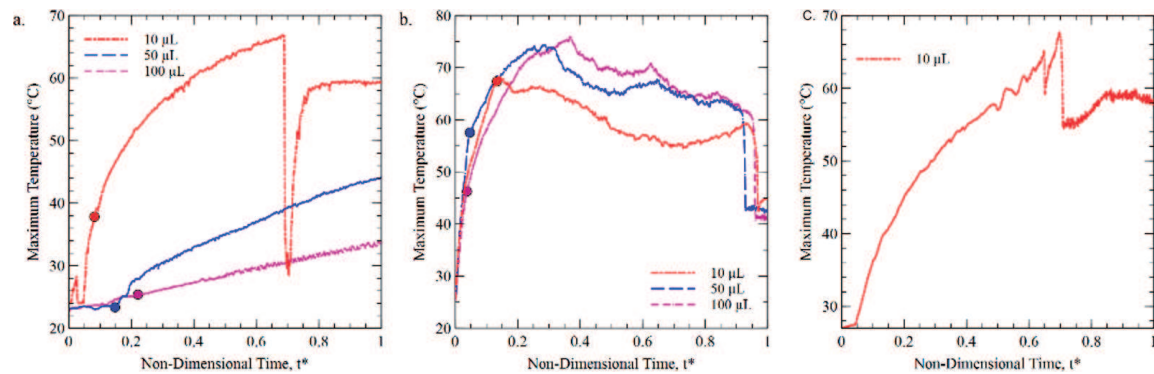


Figure 7.
The maximum temperature of liquid on the surface of (a) transducer A, (b) transducer B and (c) transducer C, extracted from the IR images recorded during liquid atomization [11].

Initial volume (μL)	Process time, t_o (s)		
	Transducer A	Transducer B	Transducer C
10	3.29	157.33	31.83
50	3.23	248.67	—
100	2.43	265.00	—

Table 3.
 Summary of the total process time for different droplet volumes on transducers A, B and C [11].

Droplet volume (μL)	Non-dimensional time (t^*)	Threshold temperature ($^{\circ}\text{C}$)
10	0.13	67.4
50	0.05	57.5
100	0.04	46.3

Table 4.
 Threshold temperature and non-dimensional time at which atomization was induced on transducer B [11].

the peak value and then went down sharply. After that process, the temperature increased again and then kept stable. However, for 50 and 100 μL droplet, the temperature just showed the increase in the whole process in **Figure 7a**. And the maximum temperature was much smaller than that of the 10 μL droplet on transducer A. As discussed before, $F_o > F_s$, the droplets could be burst out on transducer A immediately after the transducer was actuated. Meanwhile, the temperature on transducer A kept stable in this tiny time interval as shown in **Figure 7a**. After that the temperature increased due to the viscous dissipation.

For the transducer B in **Figure 7b**, $F_o < F_s$ when the transducer was turned on, the water droplet just vibrated continuously on the transducer B. And because of viscous energy dissipation, the temperature of the droplet went up quickly during the droplet vibrations as shown in **Figure 7b**. When the temperature on transducer B reached a peak value, the droplet on transducer B began to break up. As discussed before, this was because the surface tension of water (σ) decreased with the increase of temperature (T) and $F_s < F_o$. Meanwhile, when the secondary droplets were burst out, the temperature on transducer B decreased continuously.

For the droplet 10 μL on the transducer C, $F_o > F_s$ when the transducer was turned on, large amounts of droplets were jetted out. At this small time interval the temperature on transducer C kept stable, which was similar to the thermal response of the 10 μL droplet on transducer A.

4. Ultrasonic drying behavior of fabric under continuous driving

The baseline dewatering time of fabrics was determined by thermally drying two different saturated fabrics (F-1 and F-2) with the size $4 \times 4 \text{ mm}^2$ at 80°C (**Figure 8**). The saturation volumes for the $4 \times 4 \text{ mm}^2$ fabrics, F-1 and F-2, were ~ 6.45 and $\sim 8.55 \mu\text{L}$ respectively. It was observed that the water content in a given fabric (via thermal evaporation) varied linearly with time (**Figure 8**), since it was directly related to the amount of water stored in the fabric.

Figure 9 demonstrates the drying characteristics of saturated fabrics F-1 and F-2 on transducers A, B, and C. The fabric size was selected such that the sample area did not exceed the working area of the transducers. It was seen that water

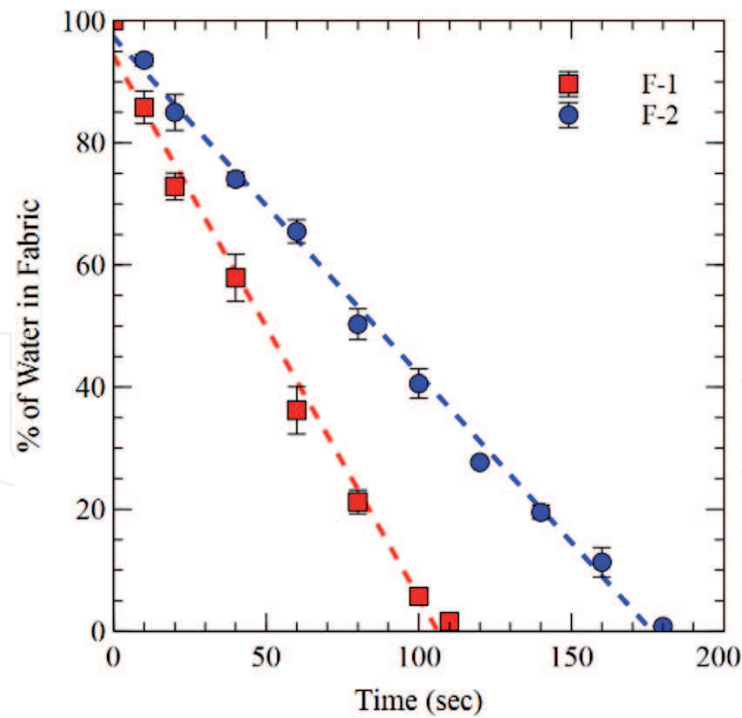


Figure 8.
Thermal drying behavior of two different fabrics [11].

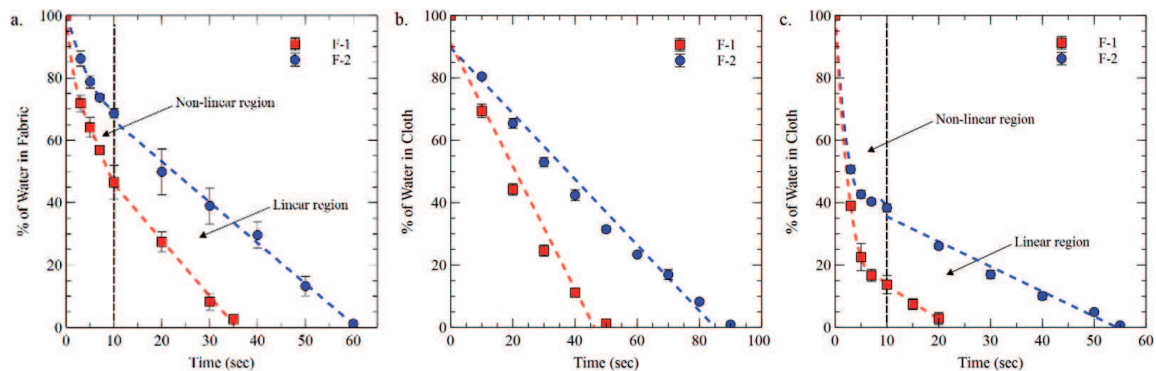


Figure 9.
Drying behavior of different types of fabric on (a) transducer A, (b) transducer B, and (c) transducer C [11].

shedding via ultrasonic excitation dewatered fabrics quicker than thermal drying (**Figure 8**), with up to an 82% reduction in drying time for fabric F-1 on transducer C. The data in **Figure 9** show that the drying curve for each fabric on transducers A and C consist of two distinct regions (indicated by the arrows in **Figure 9**):

- An initial region where the water content in the fabric decreases non-linearly with time;
- A second region where the water content in the fabric decreases linearly with time.

These two regions of the drying curve arise due to the impact of the two major forces involved in the water shedding process—the oscillation force (F_o) and the surface tension force (F_s). There are two kinds of pores in the fabrics: the large pores between the fabric threads and the small pores within the fabric threads (**Figure 4**). Due to the pore size distribution in the fabric, the surface tension force (F_s) in the fabric spans a range of values—large pores in the fabric generate low F_s while small

pores generate large F_s . At $t^* = 0$, the oscillation force generated by the transducer surface (F_o) was sufficiently large to overcome the surface tension forces (F_s) in the larger pores of the fabric, resulting in rapid shedding of water from these pores. The shedding of a large fraction of water via ultrasonic excitation resulted in a non-linear decrease in the fabric water content. The fraction of water shedding in this region was dictated by the fraction of pores in the fabric with $F_o > F_s$, with the amount of water shedding increasing as the number of such pores increase. Based on the data presented in **Figure 9**, it can be deduced that fabric F-1 consist of a larger fraction of pores with $F_o > F_s$ than fabric F-2, resulting in a greater decrease in water content during the initial non-linear phase. This conclusion can also get the evidence from **Figure 4**, which fabric F-2 shows denser structure and smaller pores compared with fabric F-1. At the end of the non-linear phase, the only pores containing liquid were those with $F_s > F_o$. The continued excitation of the transducer surface caused the temperature of liquid trapped in these pores to rise via viscous dissipation without shedding water from the fabric. This response was similar to the thermal response of droplets observed when $F_s > F_o$. The increase in temperature of the liquid (and the fabric) induced thermal evaporation from the fabric, which caused a linear decrease in the fabric water content (similar to the trend presented in **Figure 8**).

Here, the kinematics of fabric drying on transducer B were similar to those of droplet atomization, where $F_s > F_o$ at $t^* = 0$. Therefore, the primary response of the liquid upon excitation was thermal, and the fabric temperature rapidly increased due to viscous dissipation. However, since the surface tension force (F_s) in the fabric was much greater than that of the 10 μL droplet, the increase in temperature did not cause F_s to decrease below F_o . Therefore, ultrasonic drying was not induced on this transducer, resulting in the absence of a non-linear drying region. Compared with the thermal drying curves for different fabrics (**Figure 8**), it also indicates that the water shedding on transducer B was primarily driven by thermal evaporation. As in the case of thermal drying, the drying time of the F-1 fabric was shorter than that of the F-2 fabric.

In addition, the drying data suggest that a larger volume of water was shed from the fabric during the nonlinear regime on transducer C than on transducer A and, overall, fabrics dried more quickly on transducer C than on transducer A and B.

5. Ultrasonic drying behavior of fabric under burst-mode driving

A simple analysis of the dynamics of the contact between the fabric and ultrasonic transducer during the fabric drying process illustrates that the transducer does not need to be constantly on to obtain the same drying effect. As the transducer vibrates, it pushes the fabric upward. The fabric loses contact with the surface of the transducer. After some time, the fabric falls back onto the transducer due to the gravity. During the time when there is no contact between the fabric and the transducer, power is consumed with no contribution to the fabric drying [12]. Therefore, power can be supplied to the transducer in bursts rather than continuously without affecting the drying process, which can increase the energy efficiency.

The drying behavior of fabric F-1 at different duty cycles for a given modulating frequency on transducer C is presented in **Figure 10**. The fabric size was fixed at $4 \times 4 \text{ mm}^2$ and the initial water mass was 10 mg. The modulating frequency in **Figure 10a–b** is 100 and 1000 Hz, respectively. The drying behavior of the fabric with the modulating signal added keeps the same with the drying behavior of the fabric without modulating signal (represented by “No DC” in **Figure 10**), as illustrated in **Figure 10**. The total drying time increased from 20 to 30 s when the duty cycle was 20%. However, when the duty cycle was 40%, the drying time was 25 s and was 5 s less than the total drying time when the duty cycle was 20%, as

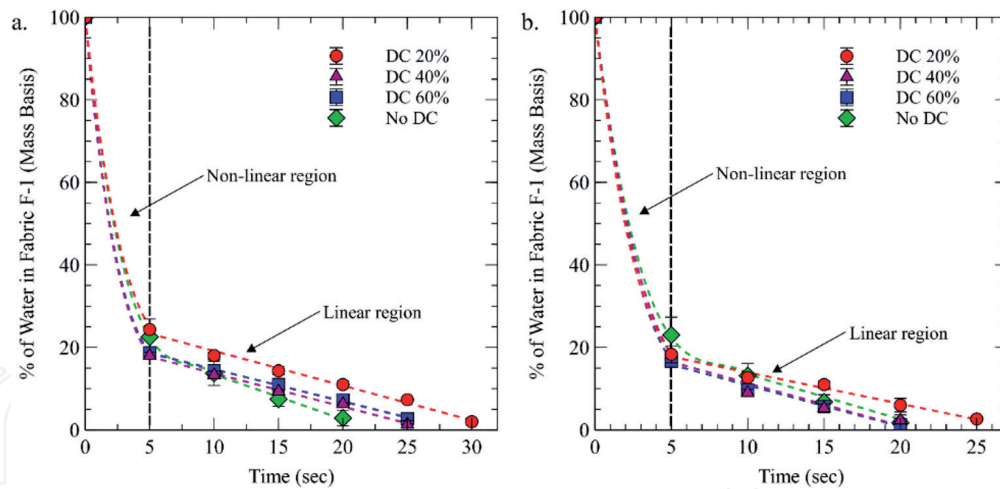


Figure 10.

Effect of duty cycle (DC) on the drying curves of fabric F-1 on transducer C. Modulating frequency: (a) 100 Hz and (b) 1000 Hz [12].

illustrated in **Figure 10(a)**. Increasing the duty cycle from 20 to 60% did not significantly affect the total drying time of the non-linear region of the drying curve. However, the slope of the linear region of the drying curve changed when the duty cycle was below 40%, resulting in an increase in the drying time.

When the transducer was turned on, because the ultrasonic excitation force of transducer C was much larger than the surface tension force of water in the large pores (i.e., $R > 1$), regardless of the duty cycle, the water accumulated in the large pores could be ejected quickly. However, water accumulated in the small pores experienced a larger surface tension force than the ultrasonic excitation force ($R < 1$). Therefore, the non-linear region of the drying behavior corresponded to water removal from the large pores while the linear region corresponded to drying in the small pores. In addition, in **Figure 10(a)**, it illustrates that adding the duty cycle did not change the nonlinear region of the drying process, but it changed the linear region of the drying process. This is also because the water embedded in the larger pores was easier to be atomized immediately after the transducer was actuated. As illustrated in **Figure 10(a)**, compared with the drying time in the nonlinear region, the drying time of the linear region was 3 times of that in the nonlinear region which there was no duty cycle added although the water percentage in the linear region was just 25% of the nonlinear region. For the duty cycle added, the linear region took even longer time compared with no duty cycle added. This is because the power in this situation was not continuously turned on and was determined by the duty cycle. The water in the fibers was even harder to be taken out by the atomization effect than the situation when there was no duty cycle. From the above analysis, it can be concluded that the duty cycle did not affect the water accumulated in the larger pores, but it affected the water accumulated in the small pores. These conclusions can also be arrived from **Figure 10(b)**.

As can be seen from **Figure 10**, it illustrates that when the duty cycle increased from 20 to 40%, the drying time decreased. The drying time also changed when the duty cycle kept the same but the modulation frequency changed. Such as, when the duty cycle was 20%, the drying time was 30 s at 100 Hz modulation frequency, but at 1000 Hz modulation frequency the drying time was 25 s. Therefore, both the duty cycle and modulation frequency of the modulating signal affected the drying time of the fabric.

The effects of different duty cycles and modulating frequencies on the drying time of a $4 \times 4 \text{ mm}^2$ swatch of fabric F-1 on transducer C is presented in **Figure 11a**. The initial water mass was fixed at 10 mg. At a 100% duty cycle, the drying time was 20 s, irrespective of modulating frequency (**Figure 11a**). This value is identical to the drying time obtained when the transducer was continuously driven. The results here

demonstrate that the drying time cannot be decreased by changing the duty cycle; however, the power consumed by the transducer can be lowered by doing so [12].

To understand the effects of duty cycle and modulating frequency on fabric drying times, the drying time of a $5 \times 5 \text{ mm}^2$ swatch of fabric F-1 was also studied on transducer C. The initial water mass was fixed at 15 mg. The results of these experiments are presented in **Figure 11b**. The results demonstrate that reducing the modulating frequency increased the drying time of fabric [12]. Furthermore, at a given modulating frequency, the drying time decreased as the duty cycle was increased up to a duty cycle D_0 . Increasing the duty cycle beyond this value of D_0 did not change the drying time. The results also indicate that the value of D_0 is dependent on the modulating frequency, such that D_0 increased as the modulating frequency decreased. As shown in **Figure 11b**, $D_0 = 60\%$ for a modulating frequency of 1000 Hz, and $D_0 = 80\%$ for a modulating frequency of 700 Hz. This implies that at a given modulating frequency, the energy consumption can be reduced without affecting the drying time by operating the transducer at a duty cycle D_0 .

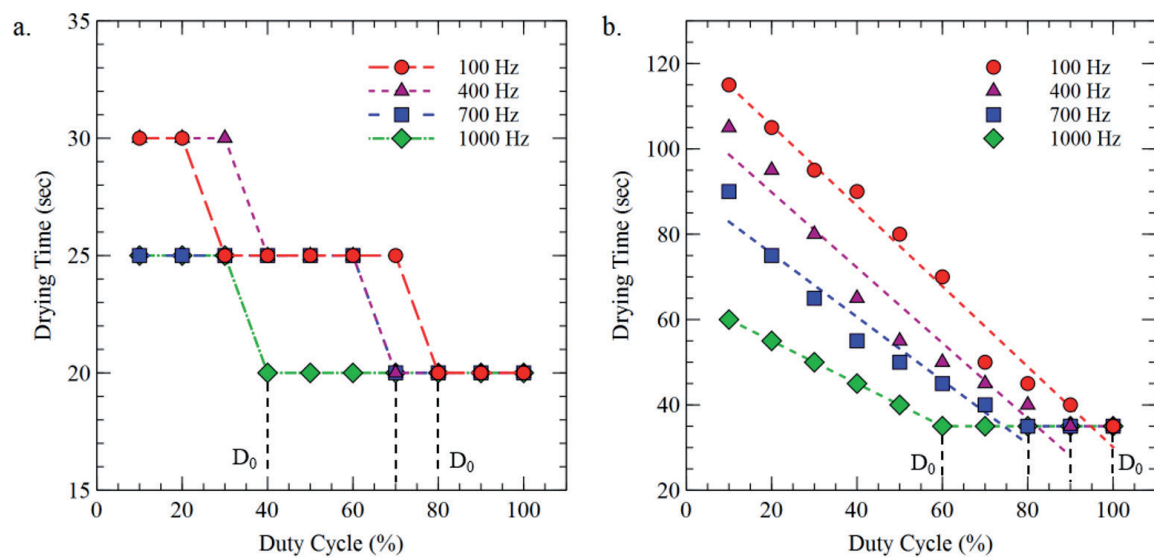


Figure 11. Effects of duty cycle on the drying time of fabric F-1 on transducer C. Fabric size: (a) $4 \times 4 \text{ mm}^2$ and (b) $5 \times 5 \text{ mm}^2$ [12].

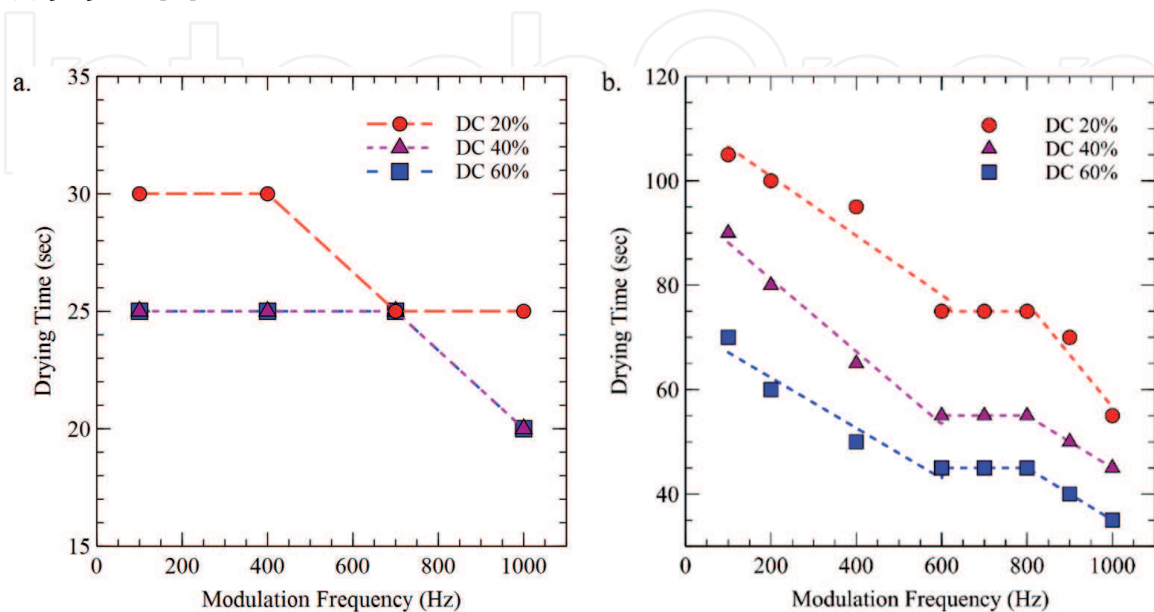


Figure 12. Effects of modulating frequency on the drying time for fabric F-1 on transducer C. Fabric size: (a) $4 \times 4 \text{ mm}^2$ and (b) $5 \times 5 \text{ mm}^2$ [12].

The effects of modulating frequency on the drying time of a 4×4 and a 5×5 mm² swatch of fabric F-1 on transducer C are presented in **Figure 12a–b**. The initial water mass for the 4×4 and 5×5 mm² pieces of fabric were 10 and 15 mg, respectively.

As seen in **Figure 12a**, since the difference of drying times at different modulation frequencies were relatively small, such as for the duty cycle 40%, the drying time at 100 Hz modulating frequency was 25 s and at 1000 Hz modulating frequency the drying time was 20 s, the drying time kept the same at certain modulating frequency. But following that modulating frequency, the drying time decreased linearly with the increase of the modulating frequency. Also, **Figure 12b** illustrates that the drying time reduced with the increase of modulating frequency. These conclusions can also be derived from the data in **Figure 11**.

6. Energy efficiency analysis

The EF ($EF_{100-20\%}$) values for the drying of fabric F-1 at different drying conditions were compared (**Table 5**). The duty cycle and modulating frequency corresponding to each drying condition are shown in **Table 5**. Drying type A refers to fabric F-1 drying on transducer A; drying types C1–C5 refer to fabric F-1 drying

Drying types	Duty cycle (%)	Modulating frequency (Hz)	$EF_{100-20\%}$ (lb/kWh)
A	Continuous driving mode		0.27
C1	Continuous driving mode		2.79
C2	10	100	19.01
C3	10	400	19.01
C4	10	700	26.61
C5	10	1000	44.35

Table 5. Comparison of energy factors (EF) for drying fabric F-1 at different drying conditions [12].

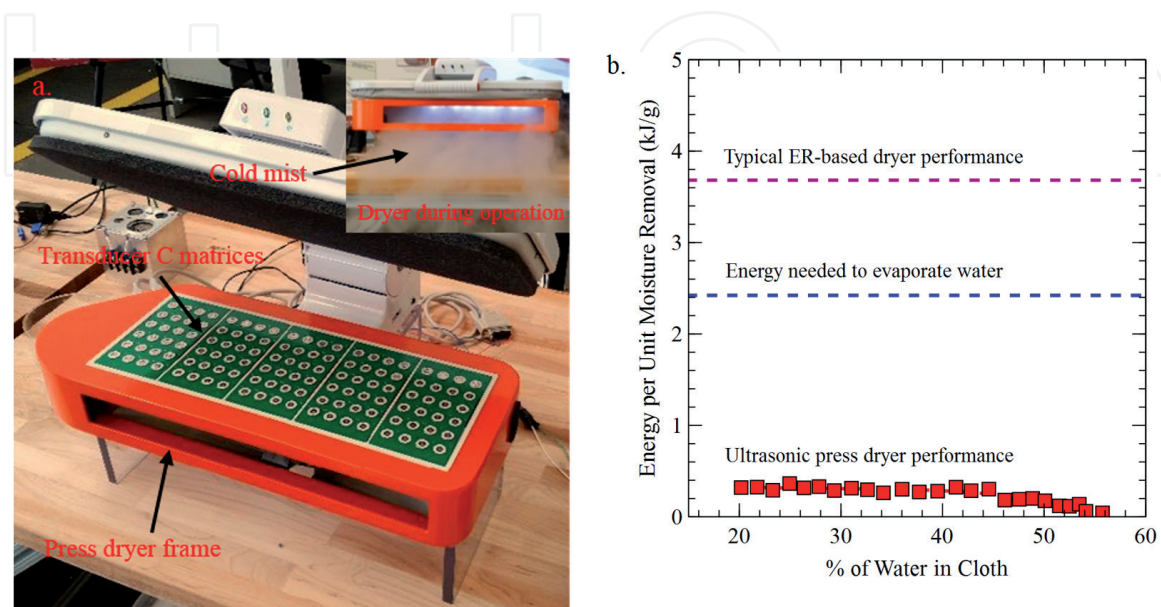


Figure 13. (a) A mid-scale press type ultrasonic clothes dryer, and (b) its energy consumption data at different initial water content [11].

on transducer C. As illustrated in **Figures 11** and **12**, the drying time for fabric F-1 dropped with an increase in the modulating frequency and duty cycle up to D_0 . The $EF_{100-20\%}$ values at different modulating frequencies with the duty cycle fixed at 10% (shortest duty cycle in the tests) were calculated and compared with continuous transducer driving (**Table 5**). The values in **Table 5** show that $EF_{100-20\%}$ values for the new drying method with modulating signals are about 7–16 times greater than those for continuous transducer driving.

A mid-scale press type ultrasonic cloth dryer was designed and fabricated, for which the ultrasonic transducer C was utilized due to its best drying performance among all the three transducers. **Figure 13a** shows the demonstration unit of this ultrasonic press dryer, which a shirt size cloth can be dried by this unit. The energy consumption per unit mass of water content (kJ/g) removed from the fabric by this ultrasonic press dryer was tested. The energy efficiency of it was compared with the latent heat of evaporation for water (at ambient temperature and pressure) and the typical electric resistance (ER)-based dryer (**Figure 13b**). The results show that the energy efficiency of the ultrasonic drying process is much higher than the thermal evaporation and ER-based drying method. Compared with the typical ER-based dryer, the energy efficiency of this ultrasonic press dryer is more than 10 times higher.

7. Conclusion

In this chapter, high-frequency, direct-contact vibrational drying of fabrics using ultrasonic transducers have been introduced as a promising technology to reduce both the drying time and energy consumption of the drying process. The physical mechanism of fabric drying was comprehensively analyzed. The results showed that the fabric drying processes consist of nonlinear and linear regimes, which were dominated by ultrasonic vibration and thermal evaporation, respectively. The electric power could be supplied to ultrasonic transducer in burst mode rather than continuously, saving energy but not affecting the drying processes. Operating the transducer on a shorter duty cycle and at a higher modulating frequency was more energy-efficient for fabric drying. Based on the initial tests on a press type ultrasonic clothes dryer, this direct-contact ultrasonic drying technique showed energy efficiency more than 10 times higher than a typical electrical resistance dryer, and 5 times higher than the latent heat of evaporation at water content greater than 20%.

Acknowledgements

The author would like to express sincere gratitude to Prof. Saeed Moghaddam in Department of Mechanical and Aerospace Engineering, University of Florida, for his support during the research work in University of Florida.

The author also would like to acknowledge support from Oak Ridge National Laboratory for its assistance.

Conflict of interest

The author declares that there are no affiliations with or involvement in any organization or entity with any financial interest or non-financial interest in the subject matter or material discussed in this manuscript.

IntechOpen

IntechOpen

Author details

Chang Peng* and Saeed Moghaddam
Department of Mechanical and Aerospace Engineering, University of Florida,
Gainesville, FL, USA

*Address all correspondence to: chang.peng@ufl.edu

IntechOpen

© 2019 The Author(s). Licensee IntechOpen. This chapter is distributed under the terms of the Creative Commons Attribution License (<http://creativecommons.org/licenses/by/3.0>), which permits unrestricted use, distribution, and reproduction in any medium, provided the original work is properly cited. 

References

- [1] How Much Electricity Do Appliances Use? Off Energy Effic Renew Energy. 2015. Available at: <https://energy.gov/energysaver/appliances-and-electronics>
- [2] Denkenberger D, Calwell C, Beck N, Trimboli B. Analysis of potential energy savings from heat pump clothes dryers in North America. CLASP. 2013;1-42. Available at: <http://clasp.ngo/Resources/Resources/PublicationLibrary/2013/Clothes-Dryer-Heat-Pump-Technology-Offers-Substantial-Cost-and-Energy-Savings-for-North-America>
- [3] U.S. Environmental Protection Agency. Market & industry scoping report: Residential clothes dryers. Energy Star. 2011;1-18. Available at: https://www.energystar.gov/sites/default/files/asset/document/ENERGY_STAR_Scoping_Report_Residential_Clothes_Dryers.pdf
- [4] Zegers FTS, Molenbroek EC. Field Test of Heat-Fed Washing Machines and Tumble Dryers. Utrecht: ECOFYS; 2000
- [5] Lekov A, Franco V, Meyers S. Evaluation of energy efficiency standards for residential clothes dryers in the USA. Energy Efficiency. 2014;7:133-149
- [6] Caldeira KG, Chan AK, Hyde RA, Kare JT, Myhrvold NP, Whitmer C, et al. Energy efficient dryer systems. US 9091015 B2; 2015
- [7] Lakkineni VR, Zentner MM, Anikhindi SM, Froelicher SB, Jr ON, MTB, et al. Energy efficient cycle for clothes dryer. US 8991068 B2; 2015
- [8] Martin E, Sutherland K, Parker D. Measured performance of heat pump clothes dryers. ACEEE Summer Study Energy Efficiency in Buildings. 2016;2016:1-13
- [9] Yoon C-H. Microwave clothes dryer. U.S. Patent No. 1988;4:765,066
- [10] McCarthy DE. Apparatus for drying clothes or other solids using microwave energy under reduced pressure with energy recovery while avoiding arcing. U.S. Patent Application No. 2013;13(/783):198
- [11] Peng C, Ravi S, Patel VK, Momen AM, Moghaddam S. Physics of direct-contact ultrasonic cloth drying process. Energy. 2017;125:498-508
- [12] Peng C, Momen AM, Moghaddam S. An energy-efficient method for direct-contact ultrasonic cloth drying. Energy. 2017;138:133-138
- [13] Deepu P, Peng C, Moghaddam S. Dynamics of ultrasonic atomization of droplets. Experimental Thermal and Fluid Science. 2018;92:243-247
- [14] Peng C, Moghaddam S. Energy efficient piezoelectrically actuated transducer for direct-contact ultrasonic drying of fabrics. Drying Technology. 2019;1-10
- [15] Patel VK, Reed FK, Kisner R, Peng C, Moghaddam S, Momen AM. Novel experimental study of fabric drying using direct-contact ultrasonic vibration. Journal of Thermal Science and Engineering Applications. 2019;11:021008
- [16] Jaffe B, Cook WR, Jaffe H. Piezoelectric Ceramics. New York: Academic Press; 1971
- [17] Khmelev VN, Savin II, Abramenko DS, Tsyganok SN, Barsukov RV, Lebedev AN. Research the acoustic cloth drying process in mock-up of drum-type washing machine. International Workshops and Tutorials on Electron Devices and Materials EDM—Proceedings. 2006:223-228

[18] Khmelev VN, Barsukov RV, Abramenko DS, Genne DV. Research and development of ultrasonic device prototype for intensification of drying process. International Workshops and Tutorials on Electron Devices and Materials EDM—Proceedings. 2008;235-240

[19] Patnaik A, Rengasamy RS, Kothari VK, Ghosh A. Wetting and wicking in fibrous materials. Textile Progress. 2006;38:1-105

IntechOpen